Journal of Catalysis **190,** 39–48 (2000)
doi:10.1006/jcat.1999.2714, available online at http://www.idealibrary.com on IDEAL®

Monomethyl-Branching of Long *n*-Alkanes in the Range from Decane to Tetracosane on Pt/H-ZSM-22 Bifunctional Catalyst

Marion C. Claude and Johan A. Martens[1]

Centrum voor Oppervlaktechemie en Katalyse, Departement Interfasechemie, K.U. Leuven, Kard. Mercierlaan 92, B-3001 Heverlee, Belgium

Received June 11, 1999; revised September 9, 1999; accepted September 21, 1999

Single long *n*-alkanes in the range *n*-C_{10}–*n*-C_{24} were hydroisomerized at 233° C in a fixed-bed down-flow vapor phase reactor loaded with Pt/H-ZSM-22 catalyst. The conversion was varied by varying the contact time. Up to ca. 60% conversion, the *n*-alkane molecules undergo almost exclusively a single methyl branching. In this conversion range, the distribution of positional methyl-branched isomers remains constant. The distributions of the positional methyl-branched isomerization products obtained with *n*-C_{12} and longer *n*-alkanes are typically bimodal. The first maximum in the methylalkane product distribution occurs at the 2-methyl-branched isomer. There is a minimum in the distribution at the 4-methylbranched isomer. The second maximum is broad and occurs at methyl positions at C_5–C_{11}, depending on the carbon number. These peculiar product distributions can be explained by the different pore mouth and key lock modes of physisorption of these long *n*-alkanes in pore openings of the zeolite. The physisorption enthalpies and entropies were estimated from molecular models of the positional methyluncosane isomers and a giant cluster of ZSM-22 framework having 1300 oxygen atoms. The physisorption energies are very large and dominate the reaction coordinate. The branching is always formed in that part of the chain that is residing in a pore mouth. In one favorable adsorption mode, designated as the pore mouth, the *n*-alkane penetrates partially into one pore opening only. The pore mouth mode favors branching at C_2 and is less favorable at more central positions along the carbon chain. In the second favorable adsorption mode, designated as the key lock type, the two ends of the hydrocarbon chain penetrate each into a different pore opening. This mode favors more central branching of the chain. The contribution of the key lock mode increases with increasing carbon number.

Key Words: **ZSM-22 zeolite; long *n*-alkanes; hydroisomerization; pore mouth catalysis; key lock catalysis.**

INTRODUCTION

Skeletal branching of long *n*-alkanes contained in petroleum fractions is of interest to the production of high-quality lubricants and middle distillate fuels. In the so-called isodewaxing process using Pt/SAPO-11 (1), the pour point is lowered by the introduction of a limited number of methyl branches in the long *n*-alkanes, while preserving the high quality associated with the paraffinic nature of the molecules. The SAPO-11 material belongs to the family of tubular pore zeolites with 10-membered rings or puckered 12-membered rings, which in their hydrogen form and loaded with a trace amount of noble metal have unique properties as hydroisomerization catalysts. In the hydroisomerization of *n*-alkanes with 8, 10, 12, 16, or 17 C-atoms, zeolites with such tubular pore systems and with MFI (2,3), MEL (2,3), FER (2,3), TON (3–7), MTT (3,7), AEL (1,8–13), ATO (10), or AFO (10,13,14) framework topology show a high selectivity for monomethyl branching of the carbon chains up to quite high *n*-alkane conversion levels. The branching is preferentially formed near the end of the carbon chain, viz., at the C_2 and C_3 positions. This behavior is different from that of zeolites with wider pores, such as ultrastable Y, on which multibranching and, especially, cracking are much more important (15).

The peculiar methyl branching selectivity is very pronounced in the Pt/H-ZSM-22 zeolite with TON topology (3–7) and has been attributed to the occurrence of pore mouth catalysis (5,6) or to product shape selectivity (16). Molecular models suggest that the formation of the branching in the carbon chain is catalyzed by an acid site located in a half-lobe at the entrance of the pore, where there is slightly more space than deeper inside the pore. The methyl side chain is formed on the part of the molecule located in the pore mouth, while the largest possible number of carbon atoms of the main chain is positioned deeper in the pore, where the interaction of this linear alkyl chain with the zeolite is very favorable. This pore mouth catalysis model for ZSM-22 is supported by adsorption data of linear and branched alkanes at catalytic temperatures (17) and by modeling (18) and simulation (19) of the methyl branching reaction kinetics, confirming the usage of a small fraction of the total available acid sites.

The second methyl branching in the carbon chain of alkanes was proposed to occur via another adsorption mode of the molecule on the surface of the ZSM-22 zeolite,

[1] To whom correspondence should be addressed. Fax: +(32) (16) 32 19.98. E-mail: Johan.Martens@agr.kuleuven.ac.be.

0021-9517/00 $35.00

designated as key lock (6). In the key lock mode, the alkane molecule located on the outer surface penetrates with parts of its carbon chain simultaneously into two or more pore openings.

In the present work, we investigated the skeletal branching of model *n*-alkane molecules in the range from decane (*n*-C_{10}) to tetracosane (*n*-C_{24}) on Pt/H-ZSM-22 catalyst to probe the features of pore mouth and key lock catalysis with model molecules that are substantially longer than the ones studied so far.

EXPERIMENTAL

Catalyst Sample

The ZSM-22 sample was synthesized according to (4). The as-synthesized sample was calcined first under nitrogen atmosphere for 5 h at 400° C and subsequently under oxygen for 16 h at 550° C. The zeolite powder was ammonium exchanged under reflux conditions in the presence of 100 ml of 0.5 M NH_4Cl solution per gram of zeolite. The zeolite sample was recovered by filtration, washed several times with deionized water until no chloride was detected in the wash water, and dried in air at 60° C. The dry zeolite powder was impregnated with tetraamine platinum(II) chloride, dissolved in a minimum amount of water to obtain a Pt loading of 0.3 wt%, and dried again in air at 60° C. The zeolite powder was shaped into tablets by compression between two blocks of stainless steel. The tablets were crushed and the fragments sieved to obtain catalyst pellets with diameters of 0.3–0.50 mm. Amounts of 0.5–3.0 g of catalyst pellets were placed inside a stainless steel reactor tube with an internal diameter of 1 cm and fixed between two plugs of quartz wool. The catalyst was activated in situ in the reactor by calcination under a flow of O_2 at 400° C for 1 h, followed by reduction in H_2 at the same temperature without intermittent cooling. The platinum dispersion determined by O_2 chemisorption was 46%.

Catalytic Experiments

Hydrocarbon feedstock, stored in a tank pressurized with helium at 220 kPa, was pumped with a Waters 590 HPLC pump into a vaporization chamber at 280° C, where it was mixed with a stream of hydrogen. The feedstock consisted of an *n*-alkane in the range from decane to octadecane, eicosane, docosane, or tetracosane (Janssen, purity >99%) diluted with heptane (Janssen, technical grade, 99%). The concentration of the long *n*-alkane in the mixture in the storage tank was 40, 20, 10, 2, or 1 mol%. An overview of the reaction conditions is given in Table 1. The partial pressure of hydrogen (P_{H2}) was 418 kPa, and that of hydrocarbon (P_{HC}) was 32 kPa, giving an overall $P_{H2}:P_{HC}$ ratio of 13.1. The reaction temperature was 233° C. The contact time, W/F_o, was varied by altering either the catalyst weight, W (g), or the molar flow rate, F_o (mol/s), of the long *n*-alkane at the entrance of the catalyst bed. Downstream of the reactor, the product was diluted with make-up hydrogen in order to reduce the hydrocarbon concentration in the gas mixture for the online analysis with GC. All tubes and valves in the circuit from the feed delivery to the reactor and to the GC sampling valve were heated at 280° C to avoid condensation of hydrocarbons. Downstream of the GC sampling valve, the hydrocarbon products were

TABLE 1

Reaction Conditions for the Conversion of *n*-Alkanes on Pt/H-ZSM-22

Run no.	*n*-C_n	mol% in feed[a]	$P_{n\text{-Cn}}$ (kPa)	$P_{n\text{-C7}}$ (kPa)	P_{H2} (kPa)	P_{H2}/P_{HC}	T of reaction (° C)	W/F_o range (kg s mol^{-1})
1	*n*-C_{10}	40	12.8	19.2	418	13.1	233	60–3000
2	*n*-C_{11}	40	12.8	19.2	418	13.1	233	100–2000
3	*n*-C_{12}	40	12.8	19.2	418	13.1	233	200–2000
4	*n*-C_{13}	40	12.8	19.2	418	13.1	233	400–3500
5	*n*-C_{14}	40	12.8	19.2	418	13.1	233	500–4000
6	*n*-C_{15}	20	6.4	25.6	418	13.1	233	600–3500
7	*n*-C_{16}	10	3.2	28.8	418	13.1	233	500–4000
8	*n*-C_{17}	10	3.2	28.8	418	13.1	233	600–7000
9	*n*-C_{18}	2	0.6	31.4	418	13.1	233	450–8000
10	*n*-C_{20}	1	0.3	31.7	418	13.1	233	500–7000
11	*n*-C_{22}	1	0.3	31.7	418	13.1	233	600–6500
12	*n*-C_{24}	1	0.3	31.7	418	13.1	233	600–7000
13	*n*-C_{16}	10	3.2	28.8	418	13.1	200	500
14	*n*-C_{16}	10	3.2	28.8	418	13.1	220	900
15	*n*-C_{16}	10	3.2	28.8	418	13.1	233	500
16	*n*-C_{16}	10	3.2	28.8	418	13.1	265	750
17	*n*-C_{16}	10	3.2	28.8	418	13.1	275	700

[a] The complement is heptane.

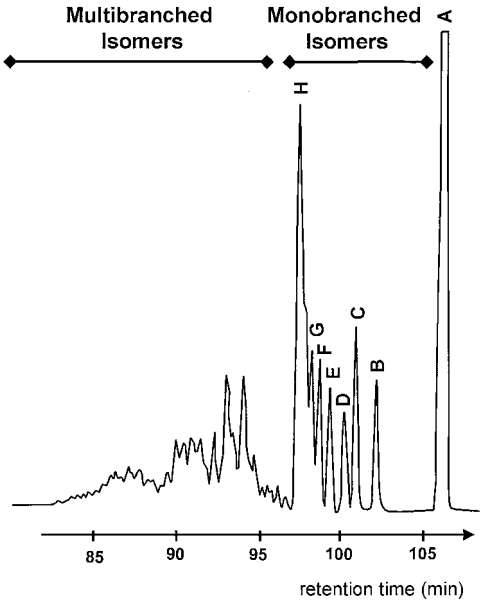

FIG. 1. Chromatogram of methyltricosanes, (A) *n*-C_{24}, (B) 3Me-C_{23}, (C) 2Me-C_{23}, (D) 4Me-C_{23}, (E) 5Me-C_{23}, (F) 6Me-C_{23}, (G) 7Me-C_{23}, (H) 8 + 9 + 10 + 11 + 12Me-C_{23}. GC temperature program: 5 min at 10° C, heating 5° C min^{-1} to 120° C, 2° C min^{-1} to 200° C, and 0.1° C min^{-1} to 205° C.

condensed in a reservoir at room temperature for eventual offline analysis.

The heptane diluent allowed us to work under realistic reaction with a relatively low $P_{H2}:P_{HC}$ ratio without using too large a heavy *n*-alkane pressure. It was also helpful to avoid the solidification of the long *n*-alkane when the unit was not in operation.

The products were analyzed online by a GC-FID (HP5880A). This instrument was equipped with a capillary column with an internal diameter of 0.32 mm and a length of 60 m (Chrompack). The stationary phase was CP-Sil-5CB and the film thickness 1.31 μm. The samples were splitless injected at a column temperature of 10° C. The column temperature programming was adapted to the molecular weight of the long *n*-alkane converted. Product identification was based on available retention indices and boiling points and identification with GC–MS (Interscience MD800 with ionization with electron impact and quadrupole m/e separator) of the condensed reaction product. The monobranched isoalkanes elute from the column as a separate group, after the multibranched isomers and before the *n*-alkane with the same carbon number. The conversion of heptane was always negligible. The chromatographic separation of the methylalkanes is illustrated for the methyltricosanes in Fig. 1.

Estimation of Lennard-Jones Adsorption Potentials with Computer Models

The 6-12 Lennard-Jones adsorption potential of alkanes on ZSM-22 was estimated using an in-house-developed software package running on a personal computer with a Pentium 166 processor. Dispersive and repulsive constants for oxygen–hydrogen and oxygen–carbon interactions in a microporous silicate were adapted from (20). These parameters give an excellent agreement between measured and calculated adsorption energies of short *n*-alkanes in ZSM-22 (21). Fragments of ZSM-22 framework represented with oxygen atoms only were generated using the crystallographic data from (22). Geometry optimization of the hydrocarbon molecule was performed using HYPERChem V 3.0 for Windows. A molecule was built using standard bond lengths and bond angles and optimized in a MM^+ force field until a rms gradient (total energy gradient calculated as a root mean square gradient) of 4×10^{-5} kJ/mol was reached. Successively, a steepest descent, a Fletcher–Reeves, and a Newton–Raphson optimization algorithm were applied. The interaction minimum was searched via a three-dimensional rotation–translation procedure using a steepest descent algorithm. Rotation and translation steps were selected in the range of 1°–180° and 0.01–0.3 nm, respectively.

RESULTS

The selectivity of monobranching isomerization, multibranching isomerization, isomerization in total, and cracking at increasing conversion of a long *n*-alkane on Pt/H-ZSM-22 is illustrated with tetracosane in Fig. 2. Based on the selectivity curves, monobranching and cracking appear as primary reactions and multibranching as a secondary reaction. The selectivity for cracking is around 10% and does not change much with conversion. The cracked products are composed of methane and ethane and the whole range of *n*-alkanes up to *n*-C_{23}, together with small amounts of isoalkanes in the C_4–C_{23} range. The formation of methane and ethane suggests that at least part of the cracking is due

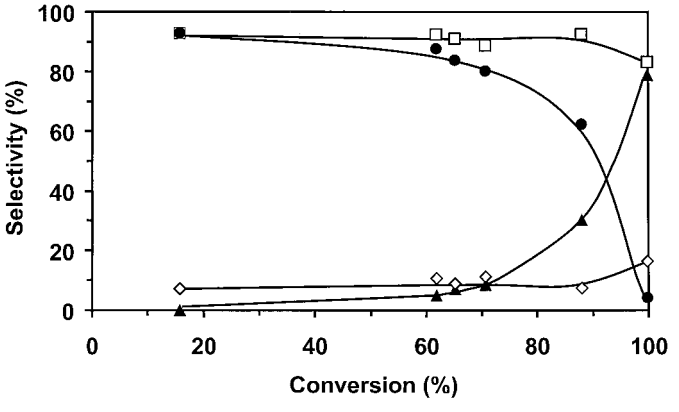

FIG. 2. Selectivity (%) for total isomers (□), monobranched isomers (●), multibranched isomers (▲), and cracked products (◇) against conversion of tetracosane (*n*-C_{24}). $T = 233$° C; $P_{H2}/P_{HC} = 13.1$. Conversion was changed by changing contact time, W/F_o, from 600 to 7000 kg s mol^{-1}.

to hydrogenolysis of the *n*-alkane on the platinum metal (23). With the other model *n*-alkanes used, the selectivity pattern is similar to the one of *n*-C_{24} shown in Fig. 2.

Up to conversion levels of 60%, the *n*-alkane undergoes almost exclusively a monobranching. Consequently, yields of monobranched isomers of the feed of 60% and more can be reached with Pt/H-ZSM-22 catalyst.

The branches in the monobranched skeletal isomers are mainly methyl groups. The chromatographic peaks of only a few ethyl-branched isomers were resolved from the large peaks of methyl-branched isomers. Their content in the monobranched isomer product fraction increases slightly with the *n*-alkane conversion level. They represent typically less than 4 mol% of the monobranched isomer fraction at high conversion. Isomers with propyl or longer side chains were not formed at all.

The initial reaction rate of methyl branching of the *n*-alkanes calculated from the initial slope of curves relating methyl branching conversion to contact time of the *n*-alkane is reported in Fig. 3. There is a decrease in reactivity from dodecane to pentadecane. The reactivity of shorter and longer *n*-alkanes does not vary substantially with the carbon number.

The evolution with conversion of the distribution of the positional methyluncosane (Me-C_{21}) isomers obtained by skeletal branching of docosane is shown in Fig. 4. Unfortunately, it was not possible to separate chromatographically the 8-, 9-, 10-, and 11-methyluncosanes. In the distributions shown in Fig. 4, the concentration of 8Me-C_{21}, 9Me-C_{21}, and 10Me-C_{21} was estimated as two-sevenths of the peak area and that of 11Me-C_{21} as one-seventh. This assumption was based on the consideration that the C_{11} carbon atom occurs only one time in the C_{21} chain, while the C_8, C_9, and C_{10} positions occur twice.

The distribution of the different methyluncosanes does not change up to 75% conversion (Fig. 4). The methyl branching of docosane occurs preferentially at C_2, followed by C_3 and positions farther down the chain. At conversions exceeding 75%, the distribution of methyluncosanes was changed significantly.

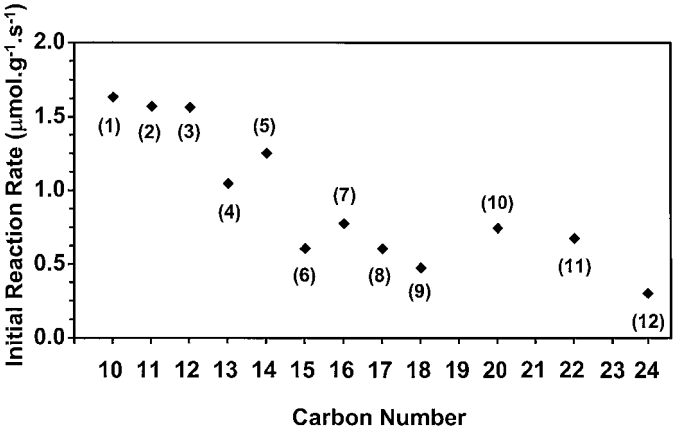

FIG. 3. Influence of *n*-alkane chain length on initial reaction rate (μmol g^{-1} s^{-1}). The numbers in parentheses correspond to the run numbers of Table 1.

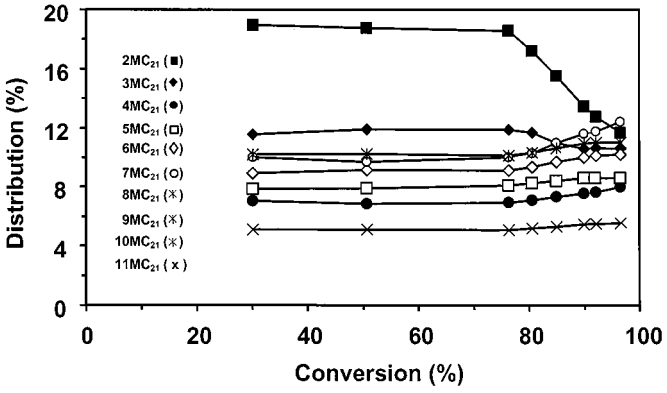

FIG. 4. Distribution of docosane (*n*-C_{22}) monomethyl-branched isomers against docosane conversion (%). $T = 233°$ C; $P_{H2}/P_{HC} = 13.1$. Conversion was changed by changing contact time, W/F_o, from 600 to 6500 kg s mol^{-1}.

The distribution of methylalkanes at 25–30% skeletal isomerization of the different *n*-alkanes is represented in Fig. 5. The C_2 position of the main chain is always preferred for carrying the methyl branching. With decane and undecane, the methyl branching preference decreases toward the center of the chain. For heavier methylalkanes, a second plateau is encountered in the distribution. The Me-C_{11} and Me-C_{12} isomers display a second maximum at C_5; the Me-C_{13} and Me-C_{14} isomers display a second maximum at C_6. For the longer chains, the second maximum in the methyl-branched isomer distribution is shifted to C_7 and farther positions. Unfortunately, the exact position of the second maximum in the Me-C_{19}, Me-C_{21}, and Me-C_{23} distributions could not be determined due to the coincidence of the relevant chromatographic peaks. Consequently, the second maximum in the distribution looks like a plateau. A minimum in the distributions occurs invariably at the C_4 position, except for the lightest alkanes investigated (Me-C_9 and Me-C_{10}), for which there is no minimum in the distribution.

Hexadecane was isomerized at temperatures of 200, 220, 233, 265, and 275° C. At each temperature, the conversion was varied by varying the contact time. At every temperature, the distribution of monomethyl-branched isomers was found to be insensitive to the conversion level below 70% conversion. The Me-C_{15} product distribution obtained at the different reaction temperatures and at ca. 50% conversion is shown in Fig. 6. The preference for branching at the C_2 position decreases with temperature at the profit of methyl branching at the C_4–C_8 positions. The content of 3Me-C_{15} in the Me-C_{15} products does not vary much with temperature.

The methyluncosanes were selected for the molecular modeling of the physisorption of heavy methylalkanes on

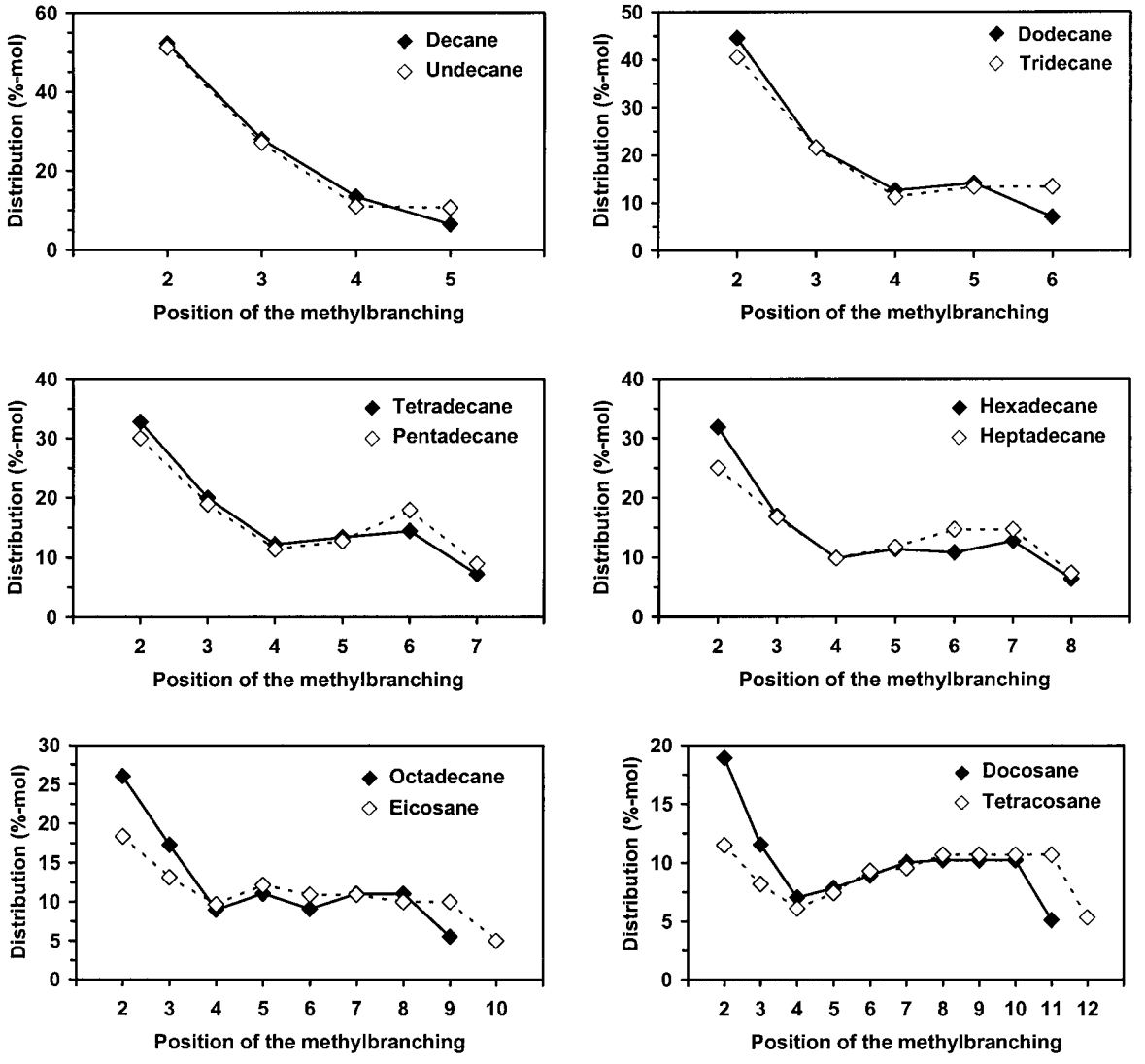

FIG. 5. Distribution (mol%) of methylalkanes isomers obtained at 25–30% skeletal isomerization of decane (n-C_{10}) to tetracosane (n-C_{24}). $T = 233^\circ$ C; $P_{H2}/P_{HC} = 13.1$.

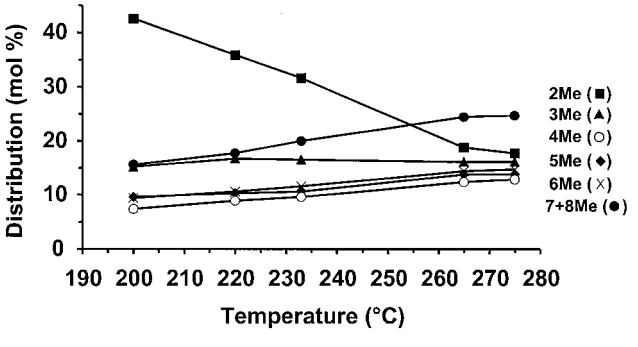

FIG. 6. Distribution (mol%) of methylpentadecanes obtained at ca. 50% conversion of hexadecane and different reaction temperatures.

the catalyst surface. The van der Waals interaction was estimated using a 6-12 Lennard-Jones potential function. The 2-Me-C_{21} molecule was built assuming standard bond lengths and bond angles and its structure optimized in vacuo. Subsequently, it was docked inside the oxygen cluster representing the ZSM-22 framework according to the pore mouth mode, with the methyl branch in the pore mouth. After position optimization, the molecule itself was optimized again inside the pore by keeping the framework oxygen atoms at fixed positions. In the next step, the position optimization routine was run another time to achieve the final optimal position of the molecule. This final situation for 2Me-C_{21} was used as a starting point for generating pore mouth models for the other positional isomers. The 3Me-C_{21} model was achieved by shortening the chain inside the pore by one carbon atom and lengthening the chain

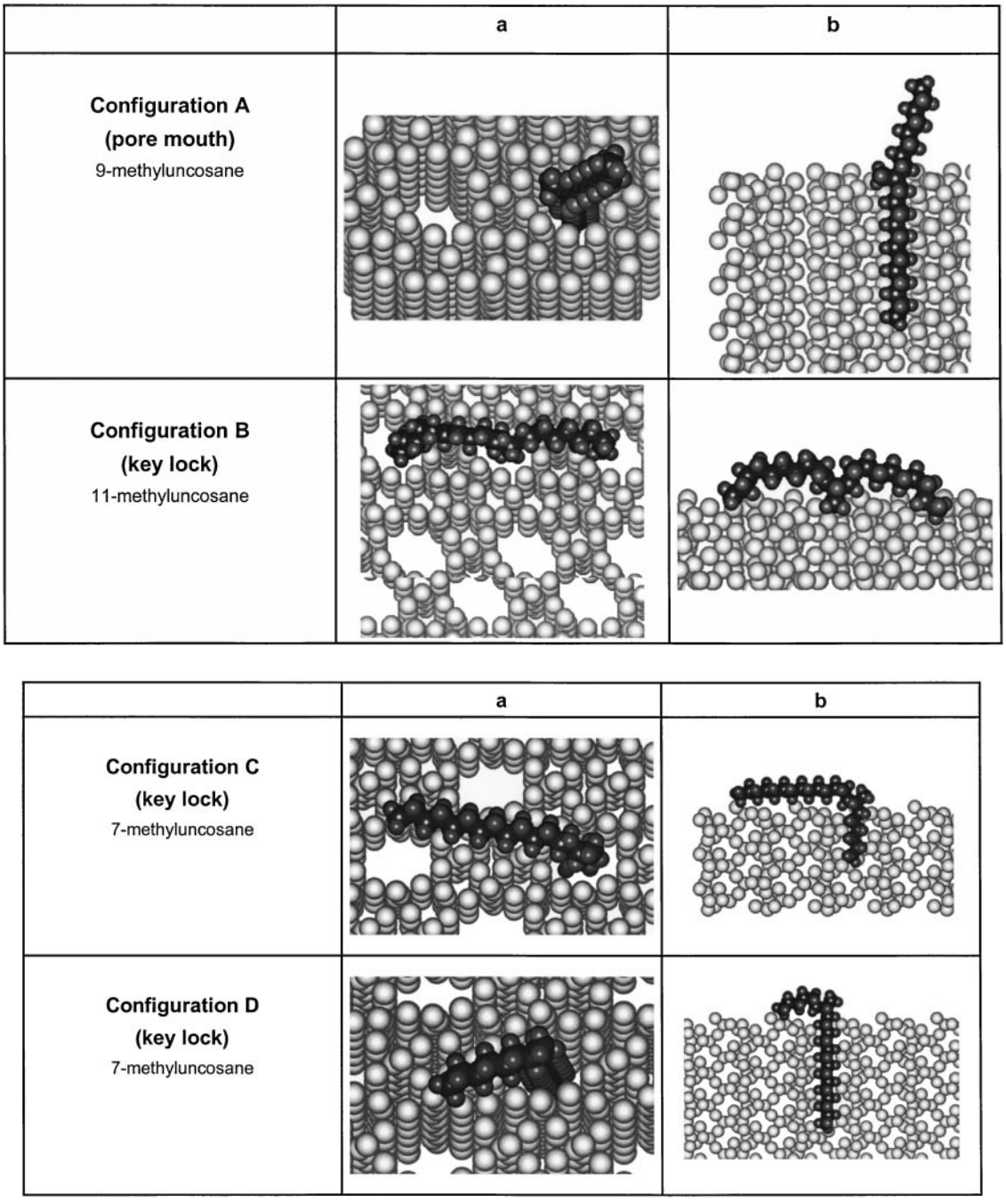

FIG. 7. Molecular models of methyluncosanes (with carbon and hydrogen atoms represented by black and dark gray spheres, respectively) in optimum interaction with a pore mouth (A) and with the smallest lock (B–F) of a ZSM-22 cluster, represented by oxygen atoms (light gray spheres).

outside the pore by one carbon. The thus obtained 3-Me-C_{21} molecule obtained was optimized first internally and subsequently with respect to its position in the zeolite. The procedure was repeated to generate all other positional isomers. The shortest part of the main chain was always located outside of the zeolite pore. The pore mouth adsorption mode will be designated as mode A in the discussions (Fig. 7).

The Me-C_{21} molecules were docked at several alternative positions on the cluster in order to find other energetically favorable positions. Five additional modes of interaction indicated with the letters B–F were found to give low potential energies. They all correspond to key lock type of adsorptions and are illustrated with specific Me-C_{21} isomers in Fig. 7.

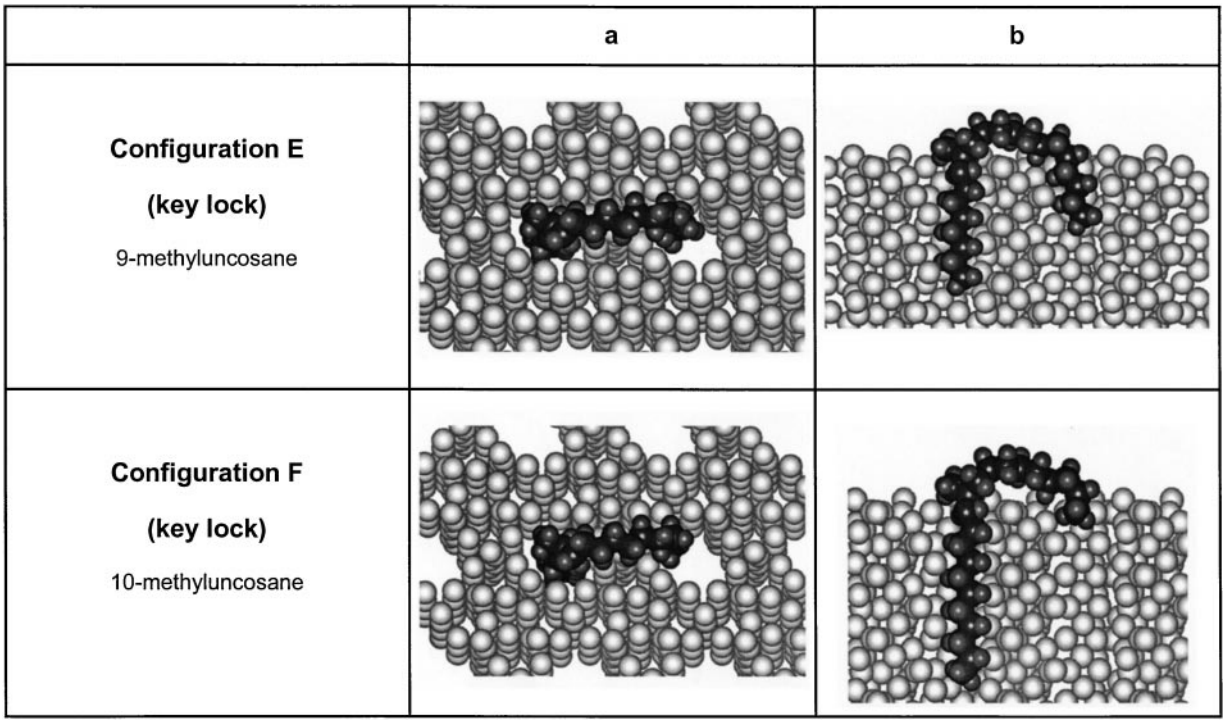

FIG. 7—*Continued*

The interaction potentials of the positional Me-C_{21} isomers at these six positions A–F are given in Fig. 8. In configuration A, corresponding to pore mouth adsorption, the interaction potential is −295 kJ/mol for 2Me-C_{21} and gradually becomes less negative the closer the methyl group is positioned to the center of the chain. In configuration B, the main chain of the methyluncosane molecule is located on the external surface exposing pore mouths. The methyl group is positioned in a pore mouth. Depending on the position of the methyl group along the main chain, one end or both ends of the main chain can also penetrate into a pore adjacent to the one in which the methyl side chain is positioned. The main carbon chain is significantly curved to allow penetration of the different parts into the pores. The potential is ca. −170 kJ/mol for 2Me-C_{21} and becomes less negative to ca. −110 kJ/mol for 11Me-C_{21} (Fig. 8). In configuration C, the main chain of the methyluncosane molecule is bent at the tertiary carbon atom. The longest *n*-alkyl chain in the molecule is stretched over the external surface, while the shortest *n*-alkyl chain penetrates into the pore. The methyl side chain is positioned in the pore mouth. The potentials in these configurations are lowest for the centrally branched isomer (ca. −180 kJ/mol). In configuration D, the largest *n*-alkyl chain is positioned inside the pore, and the shortest chain is positioned on the external surface. For the 2Me-C_{21} and 11Me-C_{21} isomers, this situation is very similar to situations A and C, respectively (Fig. 8). In configurations E and F, the main chain is bent twice to allow penetration of the hydrocarbon molecule into two pores. The distinction between configurations E and F is based on the position of the methyl group in the mouth of the pore holding the shortest or the longest alkyl chain, respectively. Especially the configuration F leads to improved interactions for chains with a methyl branching on the seventh or higher carbon atoms (Fig. 8).

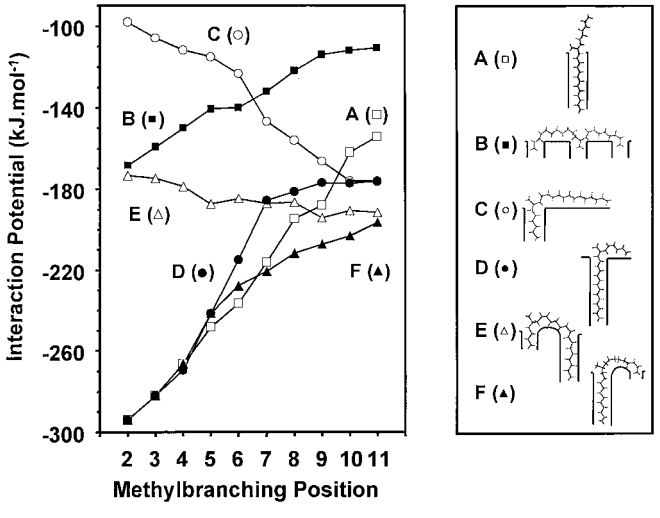

FIG. 8. Estimated Lennard-Jones 12-6 interaction potential (kJ/mol) of the methyluncosane isomers according to the pore mouth and key lock physisorption modes on a ZSM-22 zeolite cluster.

In the ZSM-22 zeolite with its narrow pores, the high adsorption enthalpy of *n*-alkyl chains is accompanied with a large loss of rotational and translational freedom (21). The adsorption entropy of the methyluncosanes was estimated by counting the number of carbon atoms positioned inside the channel and adopting the adsorption entropy values per carbon atom of short *n*-alkanes (21). At low coverage, the adsorption entropy of an *n*-alkane inside the ZSM-22 micropore, ΔS_0^θ, is given by the equation (21)

$$\Delta S_0^\theta = 15.1\ \mathrm{CN} + 36.7(\mathrm{J\ mol^{-1}K^{-1}}) \qquad [1]$$

in which CN stands for the carbon number.

The free energy change of adsorption of the positional methyluncosane isomers, ΔG_0^θ at 506 K, was calculated from

$$\Delta G_0^\theta = \Delta H_0^\theta - 560(15.1\,\mathrm{CN_{mp}} + 36.7)(\mathrm{J\ mol^{-1}}) \qquad [2]$$

in which $\mathrm{CN_{mp}}$ is the number of carbon atoms inside the micropore according to the specific configuration, and ΔH_0^θ is the adsorption enthalpy, taken as the calculated interaction potential (Fig. 8.).

The most favorable free energy of adsorption of each of the methyluncosane positional isomers is reported in Fig. 9. This estimation of free energies of adsorption shows that the Me-C_{21} isomers with methyl positions at C_2–C_6 are preferentially adsorbed according to the pore mouth mode A, while the key lock mode is preferred for the isomers with the methyl group at C_7–C_{11}. There are two minima in the adsorption free energy curve of Fig. 9 situated at the C_2 and the C_{11} positions, respectively.

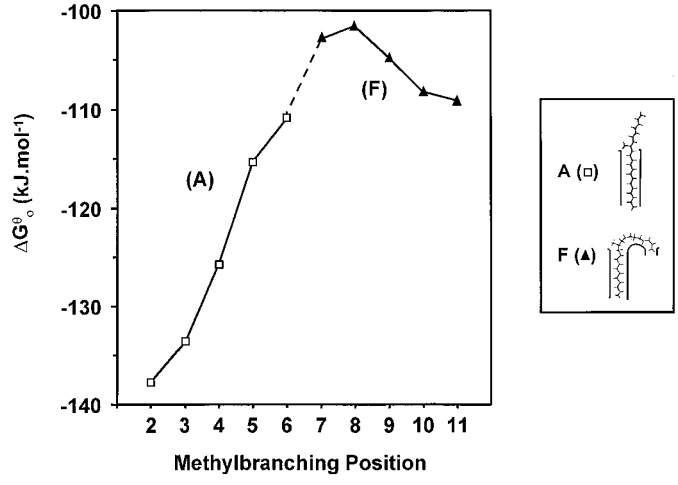

FIG. 9. Minimum free energy of adsorption, ΔG_0^θ (kJ/mol), estimated from molecular models for the different methyluncosane isomers position optimized on a ZSM-22 zeolite cluster.

DISCUSSION

The classic reaction mechanism of hydroisomerization of an *n*-alkane proceeds via several steps: (i) dehydrogenation on the noble metal; (ii) protonation of the *n*-alkene on the Brönsted acid site with formation of a secondary alkylcarbenium ion; (iii) rearrangement of the alkylcarbenium ion via the formation of cyclic alkylcarbonium type transition states; (iv) deprotonation; and (v) hydrogenation (24). Hydroisomerization of *n*-alkanes on a bifunctional zeolite is performed at relatively low temperatures, at which the reactivities of the molecules are influenced by the physisorption process (25, 26). Even for short alkanes such as hexane to nonane, reactivity differences can be pinned down to differences in physisorption energies (27). Increasing the adsorption enthalpy leads to a lower apparent activation energy and a higher reactivity. In the present work dealing with much heavier molecules, molecular modeling of the physisorption process was therefore used to find an explanation for the observed bimodal distributions of methylalkane reaction products and its dependence on the carbon number.

With the heavy alkanes and the ZSM-22 zeolite dealt with, the adsorption enthalpies are very high and reach, e.g., up to 295 kJ/mol for the 2Me-C_{21} isomer (Fig. 8). This energy represents several times the activation enthalpy for an individual reaction step such as protonation or methyl branching (28). It can be expected that the interaction potential of a molecule with as many atoms as, e.g., $C_{22}H_{46}$ is not much altered upon the introduction of a double bond, or upon protonation of this bond.

The variations of adsorption enthalpies with the position of the methyl branch in the molecule are significant (Fig. 8). These variations reflect essentially the number of carbon atoms inside and outside the pore. Similar variations must also be encountered with the reaction intermediates and transition states leading to the formation of these specific methyl positions.

The estimated free energies of adsorption of the different methyluncosanes show two optima (Fig. 9). The 2Me-C_{21} isomer is most strongly adsorbed (pore mouth mode A, $\Delta G_0^\theta = -137$kJ/mol, Fig. 9) and is the preferentially formed isomer from *n*-C_{22} at conversion levels below 80% (Figs. 4 and 5). The second adsorption optimum occurs at 11Me-C_{21} (key lock mode F, $\Delta G_0^\theta = -109$ kJ/mol, Fig. 9). Unfortunately, owing to insufficient gas chromatographic separation, it was not possible to determine the content of 11Me-C_{21} in the Me-C_{21} reaction products. The Me-C_{21} distribution obtained by equally dividing the sum of the 8Me-C_{21}, 9Me-C_{21}, 10Me-C_{21}, and 11Me-C_{21} isomers (Fig. 5) reveals that the second maximum in the distribution curve must be located among these isomers. Thus, the experimental distribution of Me-C_{21} isomers obtained by hydroisomerisation of *n*-C_{22} can be explained by the

adsorption equilibrium according to pore mouth and key lock modes. Pore mouth adsorption leads to methyl branching at the end of the carbon chain, while key lock adsorption favors methyl branching at more central positions.

The minimum at C_4 observed in the product distribution curves reflects a transition from the pore mouth (A) to the key lock (F) adsorption mode. In the free energy of adsorption curve (Fig. 9), the transition occurs between C_6 and C_7 (Fig. 9) rather than at C_4. This discrepancy can be due in part to the low calculation level used in the molecular modeling. It is also possible that the intrinsic reaction rates of branching are higher for molecules adsorbed according to pore mouth compared to key lock mode.

Up to high conversion levels such as 75% for docosane, the distribution of methyl-branched isomers does not change (Fig. 4), suggesting that methyl shifts do not occur. A similar constancy was also observed in the experiments with the other *n*-alkanes investigated in this study and with shorter *n*-alkanes in the literature (31). This is surprising as methyl shifts are known to be faster than branching rearrangements (32). The constancy of the Me-C_{n-1} product fraction is explained by the physisorption equilibrium dominating this type of catalysis. Only at long contact times (high conversions of the *n*-alkane fed to the reactor) is there internal equilibration of this fraction by methyl shift.

The contribution of pore mouth and key lock catalysis is dependent on the carbon number of the *n*-alkane. Short alkanes such as decane and undecane are converted via pore mouth mechanisms mainly, while from dodecane on, key lock catalysis starts to contribute significantly as a second maximum appears in the distribution of methyl-branched isomerization products. The contribution of key lock catalysis increases with carbon number. With the longest *n*-alkane investigated (tetracosane), the formation of 8- to 11-methylbranched isomers has become almost as important as that of the 2-methyl-branched isomer (Fig. 5).

The evolution of the reactivity of *n*-alkanes with carbon number on Pt/H-ZSM-22 catalyst is totally different from that in large-pore bifunctional zeolites. On Pt/Ca-Y, the reactivity of *n*-alkanes from *n*-C_6 to *n*-C_{11} increases significantly with carbon number (15). On Pt/US-Y, the reactivity of *n*-alkanes increases systematically from *n*-C_9 to *n*-C_{14} (29). The increase of the reactivity of the *n*-alkane with carbon number is explained by the increasing number of possible parallel reactions (30). On Pt/H-ZSM-22, a number of these parallel reactions are suppressed, depending on pore mouth versus key lock adsorption. It is striking that the step in the reactivity curve in the range from *n*-C_{12} to *n*-C_{15} coincides with the transition from almost pure pore mouth to mixed pore mouth and key lock catalysis.

The number of atoms positioned inside the pores is substantially larger in the pore mouth than in the key lock configurations, and, therefore, the adsorption entropies are smaller. Consequently, it is expected that the contribution of the key lock catalysis will increase with increasing temperature (Eq. (2)) and that the preferential formation of 2-methyl-branched isomers will decrease in favor of more centrally branched isomers. Such a tendency was observed indeed in the Me-C_{15} isomers obtained by hydroisomerization of hexadecane in the temperature range from 200 to 275° C (Fig. 6). The content of 2Me-C_{15} in the Me-C_{15} product fraction drops from 42% at 200° C to 18% at 275° C. The content of the 3Me-C_{15} isomer, which is also formed mainly through pore mouth catalysis, is less sensitive to temperature. The formation of other isomers with a more central methyl group occurs mainly through key lock catalysis and is favored at increased temperatures. The free energy gap between the pore mouth and key lock adsorptions estimated for the Me-C_{21} isomers (Fig. 9) is quite large and would not lead to such a large change in product distribution with temperature. There are probably additional factors involved, such as changes with temperature of intrinsic reaction rates of branching for molecules adsorbed according to pore mouth compared to key lock mode. The cold flow properties and the viscosity index of isoalkanes are dependent on the position of the methyl branching along the main carbon chain (33–35). Methylalkanes with the methyl group at a central position along the chain have a lower pour point compared to isomers that are methyl branched near the end of the chain. In this respect, the use of the Pt/H-ZSM-22 catalyst can be advantageous since it favors the branching of long *n*-alkanes in the center of the chain more than at the ends.

CONCLUSIONS

Pt/H-ZSM-22 is an efficient catalyst for the monomethyl branching of long *n*-alkanes in the range from decane to tetracosane. Typically up to 60% of conversion of the *n*-alkane, the composition of the methylalkane isomerization products is constant. The product distributions from dodecane and larger *n*-alkanes are bimodal with methyl branching at C_2 and at C_5–C_{12} being preferred. Molecular models suggest that these skeletal isomerizations of heavy *n*-alkanes are governed by the physisorption process. Skeletal branching near the end of the chain, and especially at C_2, occurs when the molecule is adsorbed according to the pore mouth mode. Branching at C_5–C_{12} positions occurs when the molecule is adsorbed in the key lock mode involving a penetration of the two tails in adjacent pore openings. The key lock mode is expected to be favored at high reaction temperatures, as the adsorption entropy is considerably lower than that in the pore mouth mode. These specific physisorption processes in “locks” on the external surface of the zeolite crystal are probably at the origin of additional observations, such as the decreasing reactivity with carbon

number in the range C_{12}–C_{15}, and the absence of methyl shift up to high *n*-alkane conversion levels. The use of these very long model molecules revealed that key lock catalysis also contributes to monobranching of *n*-alkanes, whereas it was previously believed to be relevant for multibranching only (6).

ACKNOWLEDGMENTS

This work is part of the Ph.D. thesis of M.C.C., sponsored by Institut Français du Pétrole (Rueil-Malmaison, France). Valuable discussions with E. Benazzi and N. Marchal from IFP are highly appreciated. J.A.M. acknowledges the Belgian government for participation in the IUAP-PAI program.

REFERENCES

1. Miller, S. J., *in* "Zeolites and Related Microporous Materials: State of the Art" (J. Weitkamp, H. G. Karge, H. Pfeifer, and W. Holderich, Eds.), *Stud. Surf. Sci. Catal.*, Vol. 84C, p. 2319. Elsevier, Amsterdam, 1994.
2. Martens, J. A., Tielen, M., Jacobs, P. A., and Weitkamp, J., *Zeolites* **4**, 98 (1984).
3. Martens, J. A., Jacobs, P. A., *Zeolites* **6**, 334 (1986).
4. Ernst, S., Weitkamp, J., Martens, J. A., and Jacobs, P. A., *Appl. Catal.* **48**, 137 (1989).
5. Parton, R., Uytterhoeven, L., Martens, J. A., Jacobs, P. A., and Froment, G. F., *Appl. Catal.* **76**, 131 (1991).
6. Martens, J. A., Souverijns, W., Verrelst, W., Parton, R., Froment, G. F., and Jacobs, P. A., *Angew. Chem., Int. Ed. Engl.* **34**, 22 (1995).
7. Ernst, S., Kokotailo, G. T., Kumar, R., and Weitkamp, J., "Proceedings, 9th International Congress on Catalysis, Calgary, 1988" (M. J. Phillips and M. Ternan, Eds.), Vol. 1, p. 388. Chem. Institute of Canada, Ottawa, 1988.
8. Jacobs, P. A., and Martens, J. A., *Pure Appl. Chem.* **58**, 1329 (1986).
9. Miller, S. J., *Microporous Mater.* **2**, 439 (1994).
10. Mériaudeau, P., Tuan, V. A., Nghiem, T. V., Lai, S. Y., Hung, L. N., and Naccache, C., *J. Catal.* **169**, 55 (1997).
11. Campelo, J. M., Lafont, F., and Marinas, J. M., *React. Kinet. Catal. Lett.* **62**, 371 (1997).
12. Campelo, J. M., Lafont, F., and Marinas, J. M., *Appl. Catal.* **170**, 139 (1998).
13. Mériaudeau, P., Tuan, V. A., Sapaly, G., Nghiem, V. T., and Naccache, C., *Catal. Today* **49**, 287 (1999).
14. Méraudeau, P., Tuan, V. A., Lefebvre, F., Nghiem, V. T., and Naccache, C., *Microporous Mesoporous Mater.* **26**, 161 (1998).
15. Weitkamp, J., *ACS Symp. Ser.* **20**, 1 (1975).
16. Webb, E. B., and Grest, G. S., *Catal. Lett.* **56**, 95 (1998).
17. Denayer, J. F., Souverijns, W., Jacobs, P. A., Martens, J. A., and Baron, G. V., *J. Phys. Chem. B* **102**, 4588 (1998).
18. Denayer, J. F., Baron, G. V., Vanbutsele, G., Jacobs, P. A., and Martens, J. A., *Chem. Eng. Sci.* **54**, 3553 (1999).
19. van de Runstraat, J. A., Kamp, P. J., Stobbelaar, J., van Grondelle, J., Krijnen, S., and van Santen, R. A., *J. Catal.* **171**, 77 (1997).
20. Pickett, S. D., Nowak, A. K., Thomas, J. M., and Cheetam, A. K., *Zeolites* **9**, 123 (1989).
21. Denayer, J. F., Baron, G. V., Martens, J. A., and Jacobs, P. A., *J. Phys. Chem. B* **102**, 3077 (1998).
22. Barri, S. A., Smith, G. W., White, D., and Young, D., *Nature* **312**, 533 (1984).
23. Sinfelt, J., *J. Catal.* **29**, 308 (1973).
24. Weisz, P. B., *Adv. Catal.* **13**, 137 (1962).
25. Steijns, M., Froment, G. F., *Ind. Eng. Chem. Prod. Res.* **20**, 660 (1981).
26. Lercher, J. A., Seshan, K., *Curr. Opin. Solid State Mater. Sci.* **2**, 57 (1997).
27. Denayer, J. F., Baron, G. V., Souverijns, W., Martens, J. A., and Jacobs, P. A., *Ind. Eng. Chem. Res.* **36**, 3242 (1997).
28. Baltanas, M. A., van Raemdonk, K., Froment, G. F., and Mohedas, S. R., *Ind. Eng. Chem. Res.* **28**, 899 (1989).
29. Debrabandere, B., and Froment, G. F., *in* "Hydrotreatment and Hydrocracking of oil fractions" (G. F. Froment, B. Delmon, and P. Grange, Eds.), *Stud. Surf. Sci. Catal.*, Vol. 106, p. 379. Elsevier, Amsterdam, 1997.
30. Weitkamp, J., *Ind. Eng. Chem. Prod. Res. Dev.* **21**, 550 (1982).
31. Martens, J. A., Parton, R., Uytterhoeven, L., Jacobs, P. A., and Froment, G. F., *Appl. Catal.* **76**, 95 (1991).
32. Brouwer, D. M., *in* "Chemistry and Chemical Engineering of Catalytic Processes" (R. Prins and G. C. A. Schuit, Eds.), p. 137. Sijthoff & Noordhoff, Rockville, 1980.
33. Brennan, J. A., *Ind. Eng. Chem. Prod. Res. Dev.* **12**, 2 (1980).
34. Needham, D. E., Wei, I. C., and Seybold, P. G., *J. Am. Chem. Soc.* **110**, 4186 (1988).
35. Briant, J., Denis, J., and Parc, G., "Propriétés rhéologiques des lubrifiants," p. 140. Editions Technip, Paris, 1985.